JOURNAL OF MATERIALS SCIENCE 13 (1978) 885–904

Microstructural characterization of "REFEL" (reaction-bonded) silicon carbides

G. R. SAWYER, T. F. PAGE
Department of Metallurgy and Materials Science, University of Cambridge, Cambridge UK

Quantitative characterization of the microstructure of a number of samples of reaction-bonded (REFEL) silicon carbide has been undertaken employing transmission and scanning electron microscopy, optical microscopy, and electron and X-ray diffraction techniques. Impurity-controlled secondary electron SEM image contrast has proved particularly useful in differentiating between the SiC present in the initial compact and that formed during the reaction-bonding process, and, in contrast to previous descriptions of the microstructure, it has been found that the newly-formed SiC is deposited from the supersaturated solution of carbon in molten silicon both epitaxially on the original SiC grains, maintaining the same α-polytypic stacking sequences, and by nucleation of fine cubic β-SiC elsewhere. The relative quantities of material occurring by these two mechanisms have been found to vary from sample to sample, although the epitaxial growth on the original grains always occurs to some extent and is responsible for the bulk cohesion of the material. Some conclusions have been drawn concerning the reaction model and the process parameters controlling the microstructure of this type of material.

1. Introduction

"REFEL" SiC* is a reaction-bonded polycrystalline high performance engineering ceramic of the type first produced by Popper [1] at BCRA, and subsequently developed by Forrest, Kennedy and co-workers [2, 3] at UKAEA Springfields, initially as a nuclear fuel-cladding material. Besides displaying a low neutron capture cross-section, good thermal conductivity and thermal shock resistance, and useful high temperature strength, the material can be made into complex shapes with sufficiently good shape tolerance on fabrication to require minimal machining of the final dense solid (see [4]). The material has also been found to have low coefficients of friction and good wear resistance when in contact with itself and various other surfaces [4, 5] and consequently, besides a number of high temperature engineering applications (see for example [4, 6, 7]), REFEL is being utilized for a variety of mechanical seals, bearings and spinnerets [4]. Thus characterization of the microstructure of REFEL materials, together with possible variations with fabrication history, and consequent control of physical and mechanical properties, is of prime interest in understanding the behaviour of this material from both a basic scientific and a technological standpoint.

The method of fabrication involves mixing an easily workable green compact of commercial 600-mesh SiC grit, colloidal graphite and polymeric binder which is shaped by traditional plastic-forming routes, heated in air to remove the binder, then caused to react in a vacuum furnace with molten silicon, which moves through the porous compact by capillary action. The increase in volume due to the transformation from graphite to silicon carbide is accommodated in the pores originally occupied by the binder. This process has been fully described by Forrest *et al.* [2], together with the coarser microstructural features of the product (e.g. the surface Si-rich

*"REFEL" is a registered trademark of UKAEA.

TABLE I Description of specimen materials

Specimen number	Forming route for green compact	Shape	SiC:C ratio in green compact* (by weight)	% of the SiC formed during reaction†	Comments
SC8B	Extrusion	Bar 25 mm × 7 mm rectangular section	2:1	62.5	
SC8R	Extrusion	Rod 5 mm diameter	2:1	62.5	
SC11	Extrusion	Cylinder with fins 17 mm o.d. 1.5 mm thick.	2:1	62.5	Fuel-can (c.1972)
SC12	Isostatic Pressing	Sheet 40 mm × 40 mm × 2 mm	4:1	45.5	
SC10	Extrusion	Rod 3.7 mm diameter	0:1	100	Specially prepared "β" sample. More than one reaction step

*[14]. (Note that a misprint in [3] implies that the SiC:graphite ratio is decreased for the pressing mix, whereas it is in fact increased from 2:1 to 4:1.).
†Calculated from the SiC:graphite ratio assuming complete conversion of all the graphite to SiC.

"burn-out" layer [1, 2]). The finer-scale microstructure has been described [1, 2] as consisting of large (~10 μm) grains of α-SiC* (present in the original green compact) bonded together by a fine matte of cubic* (β) grains formed during the reaction, with about 10% of unreacted free silicon filling the remaining porosity. The reaction mechanism [2] was deduced to be precipitation of β-SiC from a solution of graphite in molten silicon, the carbon solute being continuously replenished by mass transport down a temperature gradient in a manner similar to that reported by Beckmann [8] in his earlier work with molten silicon in graphite crucibles. These temperature gradients, in the reaction zone, are believed to be principally due to the exothermic $Si + C \rightarrow SiC$ reaction.

This paper presents the results of a microstructural study of various samples of REFEL silicon carbide undertaken as part of a wider programme aimed at elucidating the hardness, friction and wear behaviour of SiC and Si_3N_4 ceramic materials [10]. Microstructural characterization of the various commercial hot-pressed and reaction-bonded materials employed in the programme has been undertaken, as a necessary preliminary to the main study, using a combination of scanning electron, transmission electron (SEM and TEM) and optical microscopy, and X-ray diffraction techniques, and some of the results concerning the hot-pressed solids have already been reported [11, 12]. In the course of microstructural examination of REFEL SiC, unusual contrast has been observed in the secondary electron and specimen current SEM images of uncoated polished surfaces which has enabled a distinction to be made between the original SiC and that formed during the reaction-bonding process. This contrast mechanism, which is essentially purity-controlled, will be described fully elsewhere [13] and has been of critical importance in interpreting the microstructures of REFEL samples.

The current observations have been found to be incompatible with previous descriptions of the microstructure of reaction-bonded silicon carbides and new description will be presented here, together with some modifications to the previous reaction model [3].

2. Experimental

2.1. Materials

REFEL materials were obtained from standard production runs at the UKAEA pilot plant (Springfields Works, Preston) and include examples of two different routes of forming the initial mix prior to siliciding, namely, extrusion and isostatic pressing. Different SiC:graphite ratios (and hence different volume fractions of polymer binder [3, 14]) are utilized in these two routes.

*The term β-SiC refers to the cubic (3C) polytype while α-SiC refers generally to all other hexagonal (H) and trigonal (rhombohedral–R) polytypic stacking sequences. Following the Ramsdell notation [9], terminology 6H, 4H, 15R, 3C etc. will be used later in this paper to designate both the layer repeat and crystal system of particular polytypic structures.

TABLE II Concentrations of some of the major impurities in typical starting materials used for the manufacture of REFEL [14]. "Old" SiC refers to the original grit in the green compact while the "new" Sic is that formed in the reaction-bonding process.

Starting material		Impurity concentrations (p.p.m)											
		Known acceptor impurities [28]					Other principal impurities						
		Al	B	Be	Ga	In	Fe	V	Ti	Ca	Mo	Mn	Ba
"Old" SiC		130	<10		<10	<10	250	100	300	<30	<50	<10	
"New" SiC	Graphite	40						17	20	170	80	40	4
	Silicon	165	20	<2			130	<1	14	50	<15	5	20

A further special sample of REFEL, produced at UKAEA by a modified process eliminating the α-SiC from the initial compact, was also examined. SiC produced from the reaction between silicon and graphite alone had been ground and mixed with more graphite to form the starting powder for a second reaction bonding process.

Characterization of this specimen material enabled additional information to be obtained concerning the "seeding" effect of the initial α-SiC grits on the crystallography of the product. Further details of the experimental materials are given in Table I, while Table II gives chemical analyses of typical starting materials [14].

2.2. Techniques

Specimens for examination by both optical and scanning electron microscopy were prepared by sectioning with a high-speed annular diamond saw (CAPCO Q35, mark II), hot-mounting in an electrically-conducting thermosetting resin (to prevent charging in the SEM) and polishing on 220, 320, 400 and 600 mesh SiC papers for about 1 min at each stage, followed by 6.0, 1.0 and and 0.25 μm diamond impregnated cloths on aluminium wheels for 2 to 3 min at each stage. Optical micrographs of the unetched polished surfaces were taken using a Zeiss Neophot 2 photomicroscope. Specimens for SEM examination were mounted on aluminium stubs using "Durofix" and a conducting path to earth further ensured by painting a track from specimen surface to stub with "silver dag". The specimens were then examined uncoated in a Cambridge Stereoscan Mark IIA using both secondary and backscattered modes.

Area fractions of various microstructural features were estimated from positive prints of scanning electron micrographs using a Quantimet 720 B image analyser. Automatic discrimination of the various grey levels involved was found to be unreliable and hence the outlines of the features of interest were transferred onto tracing paper and shaded.

Specimens for transmission electron microscopy were prepared by cutting thin slices (~200 μm), using the CAPCO saw, from which 3 mm discs were cut using a Kerry "Sonorode 150" ultrasonic drill. These discs were mounted on a $1\frac{1}{4}$ in. diameter aluminium block using Lakeside 70 wax and polished as described above, then demounted and polished on the reverse side. The resultant discs were about 100 to 120 μm thick and were subsequently thinned to perforation using an Edwards IBMA2 ion-beam thinner (6 kV, 60 μA per gun at 20° incidence), the thin foils obtained being examined using a JEOL 200A electron microscope at 200 kV. Though perforation of these relatively thick discs takes about 48 h, the resultant thick, parallel-sided outer annulus on each specimen renders them mechanically strong for repeated insertion into the electron microscope holders. This effect was enhanced further during thinning by supporting the specimen between tantalum discs with 1.9 mm central holes rather than the more usual 2.5 mm ones. Both TEM and SEM samples could be examined without the need for any conductive coating (see Section 3).

X-ray diffractometry studies were made on flat polished sections (prepared as previously described to 0.25 μm diamond finish) using a standard Philips vertical diffractometer with a Cu$K\alpha$ line source and a paper chart output. Structure factors and expected peak positions were calculated for the most common SiC polytypes 3C, 4H, 6H and 15R, using the atomic coordinates given by Schaffer [15] and the reduced structure factor formulae from the International Tables for X-ray crystallography. Estimates of the errors in the calculated structure factors from Debye–Waller temperature corrections and small deviations from the ideal

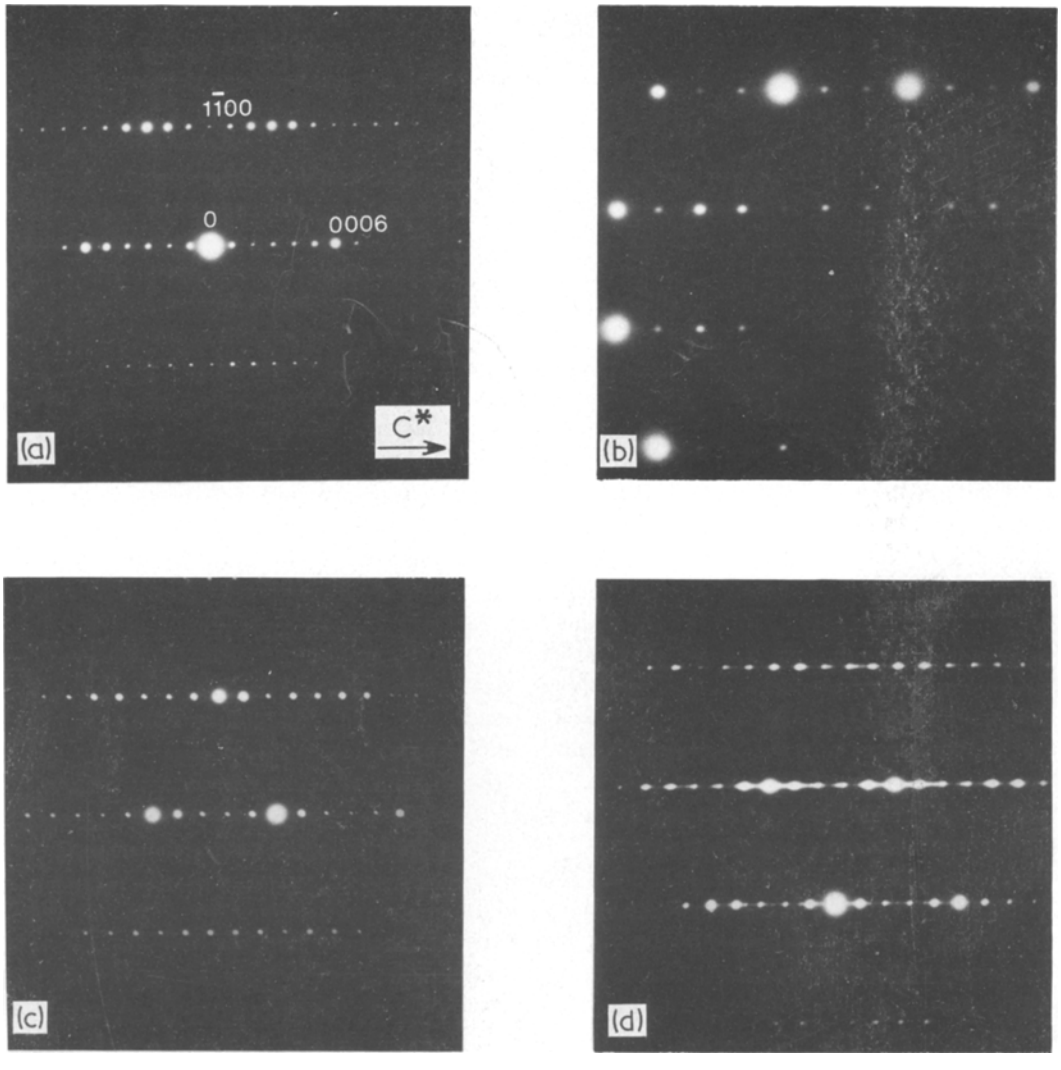

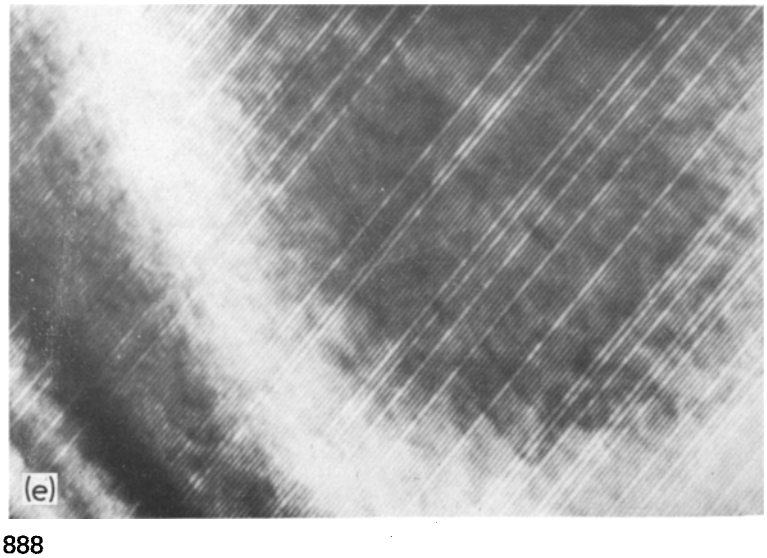

Figure 1 Selected area diffraction patterns from grains tilted such that the polytypic stacking direction lies in the plane of the pattern: (a) 6H, beam direction $[1\,1\,\bar{2}\,0]$; (b) 3C (twinned), beam direction $[1\,1\,0]$; (c) 15R, beam direction $[1\,1\,\bar{2}\,0]$; (d) faulted 15R ($[1\,1\,\bar{2}\,0]$) showing continuous streaking and extra reflections along $\langle 0\,0\,0\,1\rangle$; (e) lattice image from a 6H grain containing occasional stacking faults (o, + $g_{0\,0\,0\,1}$, + $g_{0\,0\,0\,\bar{1}}$ —symmetric diffraction conditions), the regular (0 0 0 1) fringes being 15.08 Å apart.

atomic coordinates (since the Si–C bond length is not always constant) were made for the 6H polytype using the refined data of Gomes de Mesquita [16] and found to be small (< 5%). Calculations were based on uncorrected structure factor values since similar refined data are not available for the other polytypes. Expected intensities were then calculated allowing for the different unit cell volumes of the various polytypes and ignoring double diffraction effects which occur in electron diffraction studies of this material.

For peaks experimentally recorded in the range $2\theta = 40°$ to $60°$ (which contains individual peaks from silicon and from each of the SiC polytypes except 3C, for which the peaks are superimposed on those of the 6H and 15R polytypes), integrated intensities and background counts were estimated from the chart traces and standard Lorentz polarization, absorption and multiplicity corrections made before fitting to the computed intensities. In this way, estimates were made of the volume fractions of the silicon and different SiC polytypes in the samples, the 3C intensity always being found by comparison between the overlapping peaks and those due to 6H and 15R alone. For all polytypes except 3C, several peaks occurred in the range examined, and for each polytype there was good agreement between the observed and calculated relative peak heights, with the exception of the common $1\,1\,\bar{2}\,0$ peak, which was relatively far larger than predicted. This was thought to be caused by $\{0\,0\,0\,1\}$ stacking disorder resulting in a uniform relative lowering of all peak heights except for reflections from planes in the $[0\,0\,0\,1]$ zone – i.e. anomalous absorption. This effect was also observed in X-ray diffraction traces from the β-SiC sample (see Section 4.5) in that the $2\,2\,0$ reflection was again far too large by comparison with $2\,0\,0$. All such reflections (i.e. those in the zone(s) of the stacking direction(s)) were discounted for quantitative estimates of the relative abundance of the phases present.

In addition to the bulk X-ray diffraction data, information regarding the polytype of grains in thin foil specimens was obtained by high resolution electron microscopy and electron diffraction. These techniques also allowed variations in the stacking sequence within any one grain to be determined. Within the limits of specimen rotation on standard double tilt holders, the polytype of any selected grain was determined by tilting† until the crystallographic c-axis ($\langle 0\,0\,0\,1\rangle$ or $\langle 1\,1\,1\rangle_{\text{cubic}}$) lay in the plane of the diffraction pattern. The number of doubly-diffracted (space-group absence) reflections observed to occur along c^* between the origin and the $2.512\,\text{Å}^{-1}$ fundamental layer spacing reflection is then indicative of the polytype (see Figs. 1a, b and c which show examples of the diffraction patterns corresponding to the 6H, 3C and 15R stacking sequences). Detailed stacking sequences, yielding information on the distribution and character of stacking faults commonly observed in these materials, were then determined from "lattice images" of, for example, the $(0\,0\,0\,1)$ and $(0\,0\,0\,2)$ planes of the 6H polytype (spacings approx. 15 and 7.5 Å respectively). Fig. 1d shows a typical example of the selected area diffraction pattern from a randomly faulted 15R structure (continuous streaking along c^*) while Fig. 1e shows part of the lattice image from a 6H grain containing occasional stacking faults.

3. Secondary electron impurity-sensitive constrast in the SEM

During the SEM examination of uncoated REFEL specimens, an image contrast effect has been observed which, though to be reported in detail elsewhere [13], is briefly described here since its occurrence has been critical in the interpretation of these microstructures. Backscattered (high energy or "reflected") electron SEM images of polished, uncoated REFEL specimens are relatively featureless except for some atomic number and polishing relief contrast between the Si and SiC phases, together with some occasional electron channelling contrast between the individual SiC grains. However, secondary electron images (and also specimen-current images) exhibit considerable contrast within those areas which can definitely be identified as SiC alone by comparison with both backscattered SEM images and optical micrographs (see Fig. 2). This contrast is believed to be due to the distribution of trace impurities within the SiC. The presence of certain impurities creates acceptor electron states in the band gap of this essentially covalent solid and thus lowers the secondary electron coefficient (δ), from the value characteristic of the pure material, by reducing the

†The necessary directions of tilt were determined either from diffraction patterns or extinction contours or, for those grains containing discrete stacking faults, by tilting until these $(0\,0\,0\,1)$-planar faults were viewed edge-on.

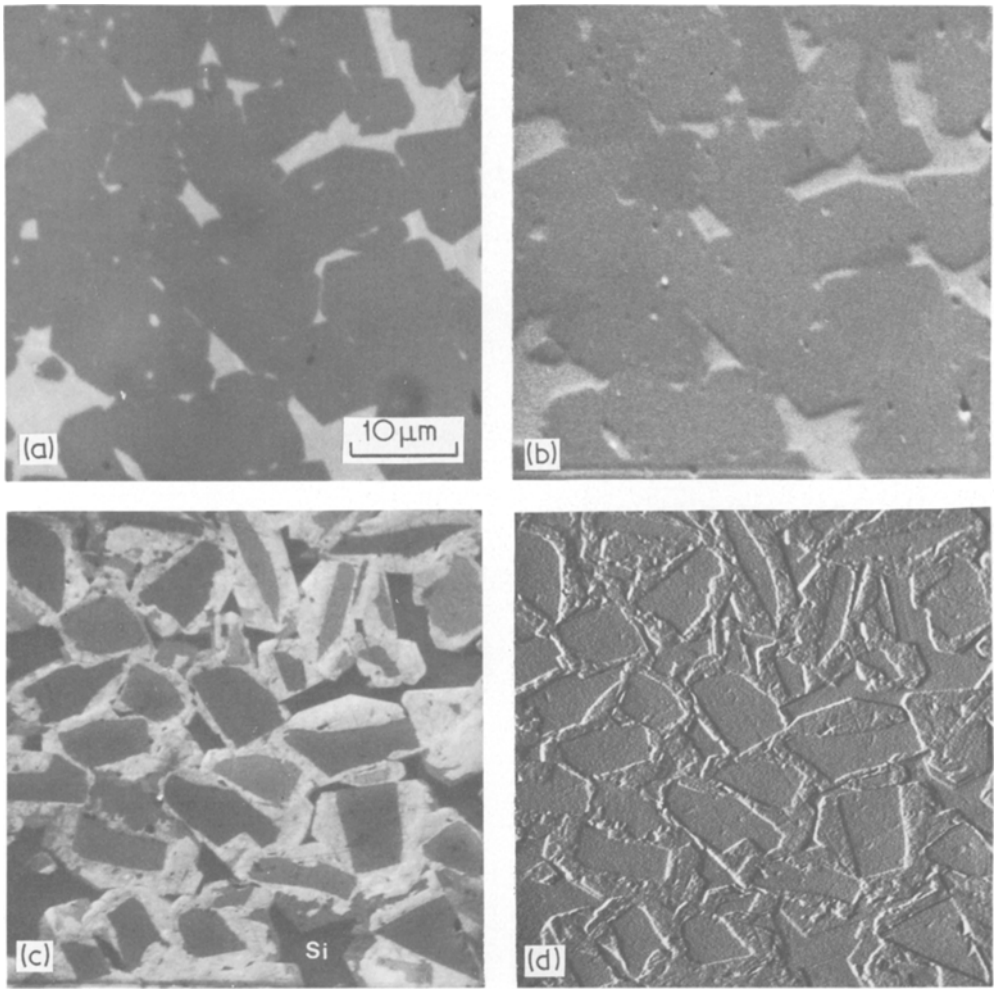

Figure 2 A series of micrographs showing the typical microstructural features of a polished sample of REFEL bar (SC8 B). Each micrograph shows the same sample area using different imaging techniques: (a) optical micrograph; (b) backscattered SEM image (10 kV) showing atomic number contrast between silicon (light) and silicon carbide; (c) secondary electron SEM image (20 kV) showing the grain structure within the SiC. The silicon now appears black and there is also contrast within each SiC grain. Some dark contrast from the SiC adjacent to residual silicon can be observed (e.g. bottom RH quadrant); (d) differentiated version of (c) revealing the uniformity of shade within the dark core of each grain.

escape probability of secondary electrons. Impurities creating donor electron states may be able to enhance δ by increasing the secondary electron supply. Thus variations in δ should be observed over the range of impurity levels immediately below that required to make the semiconductor degenerate (typically ~ 100 p.p.m. [17]), and will only be caused by soluble elements which generate extrinsic electron states in the electron energy band gap. Though such elements cannot be individually identified by such contrast, variations in their concentration can be detected with mass and spatial resolution beyond conventional X-ray microanalysis. Conductive specimen coatings completely destroy the effect since they dominate the secondary electron yield, and in the present studies all specimens were found to be sufficiently semiconducting not to require any coatings.

4. Detailed microstructural observations

4.1. Extruded bar sample (SC8 B)

Transmission electron microscopy of thin foils from this sample revealed a grain structure of relatively uniform size ($\sim 10\,\mu$m) and equiaxed morphology as shown in Fig. 3. In contrast to

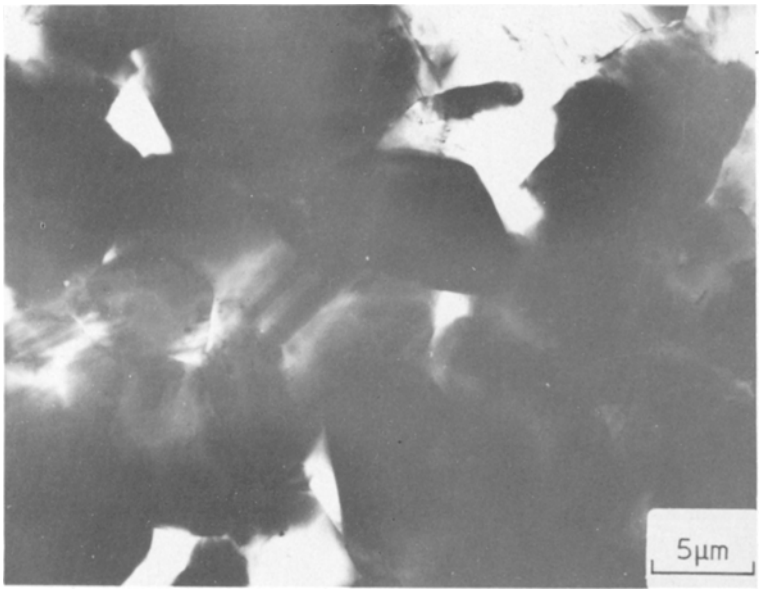

Figure 3 Transmission electron micrograph of SC8 B showing the relatively uniform size distribution of the faulted grains.

previous descriptions of the microstructure (see Section 1), there was no evidence of any fine SiC matte and electron diffraction showed that all the grains in foils of SC8 B were basically either 6H or, less commonly, 15R although some degree of disorder was common and examples of longer period repeats superimposed on these basic structures were found. In the necessarily small sample of grains examined by electron microscopy, no grains were found having an exclusively 3C structure and this agrees well with the bulk X-ray diffraction results given in Table III, which show

TABLE III X-ray diffraction data

Sample	Percentage silicon	Distribution of polytypes in the silicon carbide as a function of total volume of silicon carbide (%)					Theoretical % new SiC in total SiC (from Table I)
		6H	15R	4H	Total α	Cubic 3C	
SC8 B	15	83	11	3.5	97.5	2.5	62.5
SC8 R	12	51	7	2	60	40	62.5
SC12	29	65	9	3	77	23	45.5
SC10	not calculated	2	2	2	5	95	100
Original SiC grit	not calculated	61	12	21	94	6	0

(likely errors less than 2% of the total volume)

TABLE IV Quantitative estimates of phase distributions

Sample	Silicon (%)	Nodules containing no large grains (%)	Angular grain cores (%)			Theoretical amount old SiC in SiC (%)
			In sampled areas (excluding nodules)	In total volume	In SiC	
SC8 B	13.5	Nil	33	33	38	37.5
SC8 R	n.d.†	Nil	32.5	32.5	37*	37.5
SC12	n.d.†	15	41.5	35	50*	54.5

*Corrected using silicon percentages from X-ray measurements (Table III).
†Not determined due to fine and inhomogeneous nature of distribution.

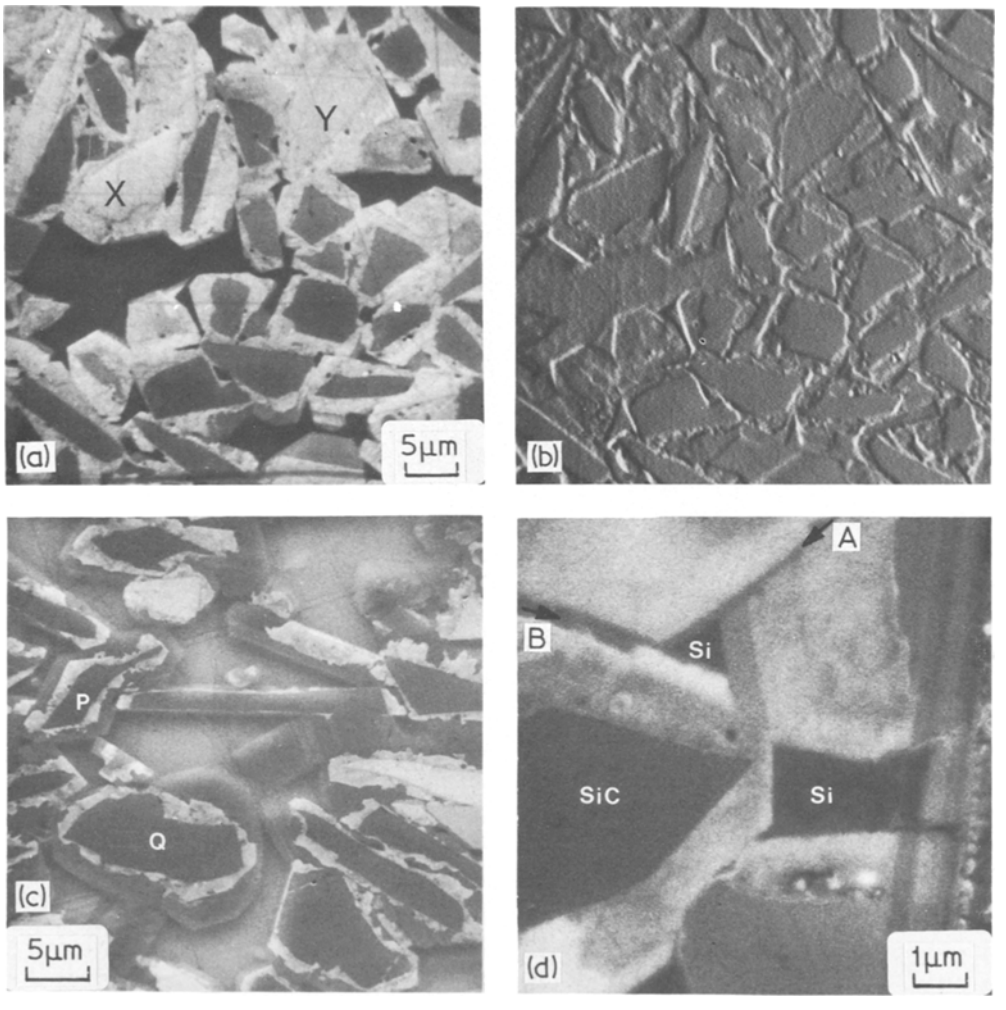

Figure 4 20 kV secondary electron SEM images from the REFEL bar (SC8B): (a) shows two light original grain cores at X, Y; (b) differential of (a) delineating the cores X and Y more clearly; (c) shows the "sandwich" structure of grains P and Q (see test); (d) a triple point between three composite grains including small areas of residual silicon. Two of the grain boundaries A and B show narrow bands of dark contrast while the third does not.

that the proportion of 3C polytype in REFEL from this sample is very small. Recent work [18] has shown further that this small amount of 3C is not present as distinct 3C grains but as occasional remnants of 3C stacking in grains which have predominantly transformed to the hexagonal (6H) structure.

Optical micrographs (Figs. 2a and 9a) revealed a fairly coarse microstructure with large masses of SiC and about 10 to 15% of free Si occupying the remaining porosity. In the SEM, a back-scattered image of the same area (Fig. 2b) shows the same general features with the silicon distinguished from the SiC both by atomic number contrast and polishing relief. The corresponding secondary SEM image (Fig. 2c) shows the grain structure within the SiC mass, and also exhibits impurity contrast within the individual grains (see Section 3). The grain structure is similar to that observed in the TEM, but each grain can be seen to have an angular core of uniform colour surrounded by a region of less uniform contrast, the boundary between the two being sharp. These different regions are well distinguished in a differentiated secondary electron image (Fig. 2d), which emphasizes the marked uniformity of the grey level in the core. The cores are nearly always dark (although occasional white examples are observed (Fig. 4)), whilst the exterior is predominantly lighter in shade,

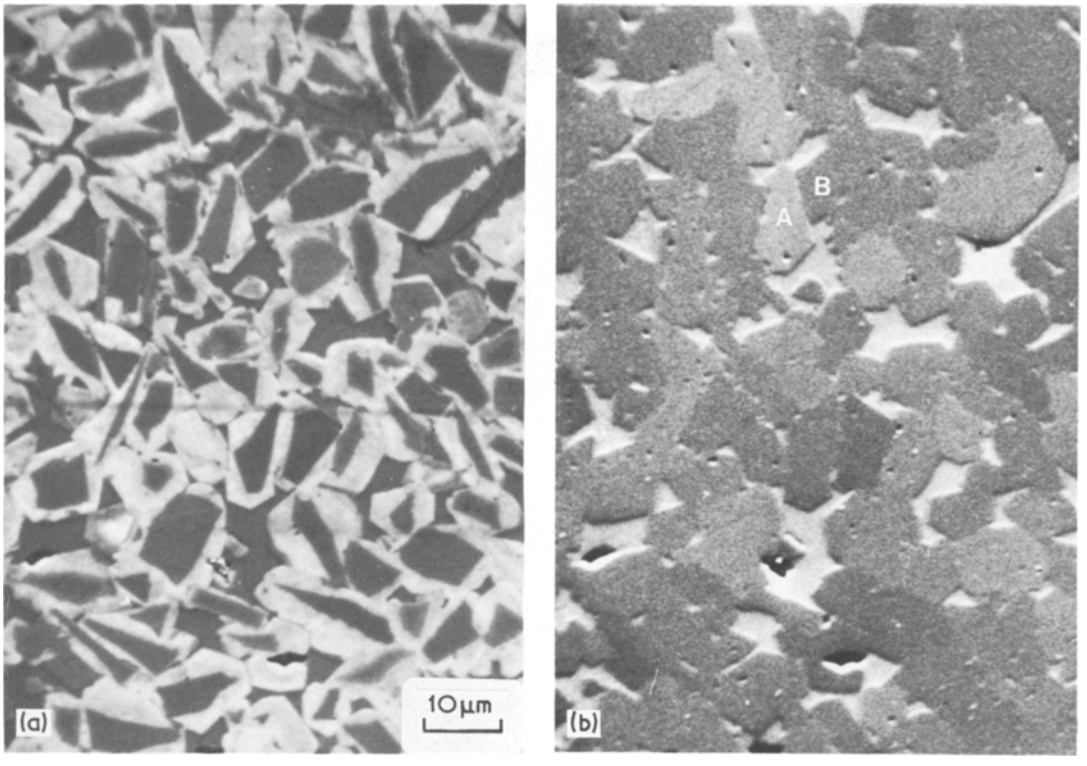

Figure 5 A pair of SEM images from the same region on a sample of SC8 B (a) a secondary electron image (10 kV) revealing the grain structure. (b) A backscattered image (10 kV) showing channelling contrast between adjacent grains. The boundary between grains A and B can be identified and each grain seen to comprise a composite in the secondary electron image.

the region immediately adjacent to the core being always white. The extreme outside of the grain, particularly where adjacent to residual silicon, is frequently dark (see Fig. 2c), and in some samples a complete outer dark layer is observed giving the appearance of a "sandwich" of light material between two dark layers (Fig. 4c). In such cases the boundary between the outer dark layer and the white layer is always sharp although often of irregular shape. This impurity-sensitive secondary electron contrast also reveals some evidence of segregation of impurities to the SiC: SiC grain boundaries, for example Fig. 4d.

In some of the backscattered SEM images, channelling contrast is visible, which allows individual grains to be distinguished on account of their different orientations, and confirms that the various regions described above are indeed parts of a single grain (Fig. 5). It should be emphasized here that the SiC grains examined by transmission electron microscopy displayed no significant variations in polytype consistent with the structures observed by SEM: however, occasional evidence of poorly-bonded SiC sub-grains of the same polytype and in exactly similar orientations were observed (Fig. 6).

Quantitative measurements of the volume fractions of silicon and angular grain cores are shown in Table IV. The volume fraction of silicon agrees well with that obtained by X-ray diffraction, and that of the angular grain cores fits well with the predicted proportion of original silicon carbide, confirming the identification of these angular grain cores with the original silicon carbide particles.

4.2. Extruded rod (SC8 R)

Optical examination of this material revealed a markedly less uniform overall microstructure than SC8 B, with some of the silicon carbide taking the form of a fine ($\sim 1\,\mu$m grain size) distribution in a silicon matrix, the distribution of this fine material showing a systematic increase from the outside to the centre of the billet (Figs. 7a and b). Secondary electron SEM images showed that the microstructure again consisted of large cored

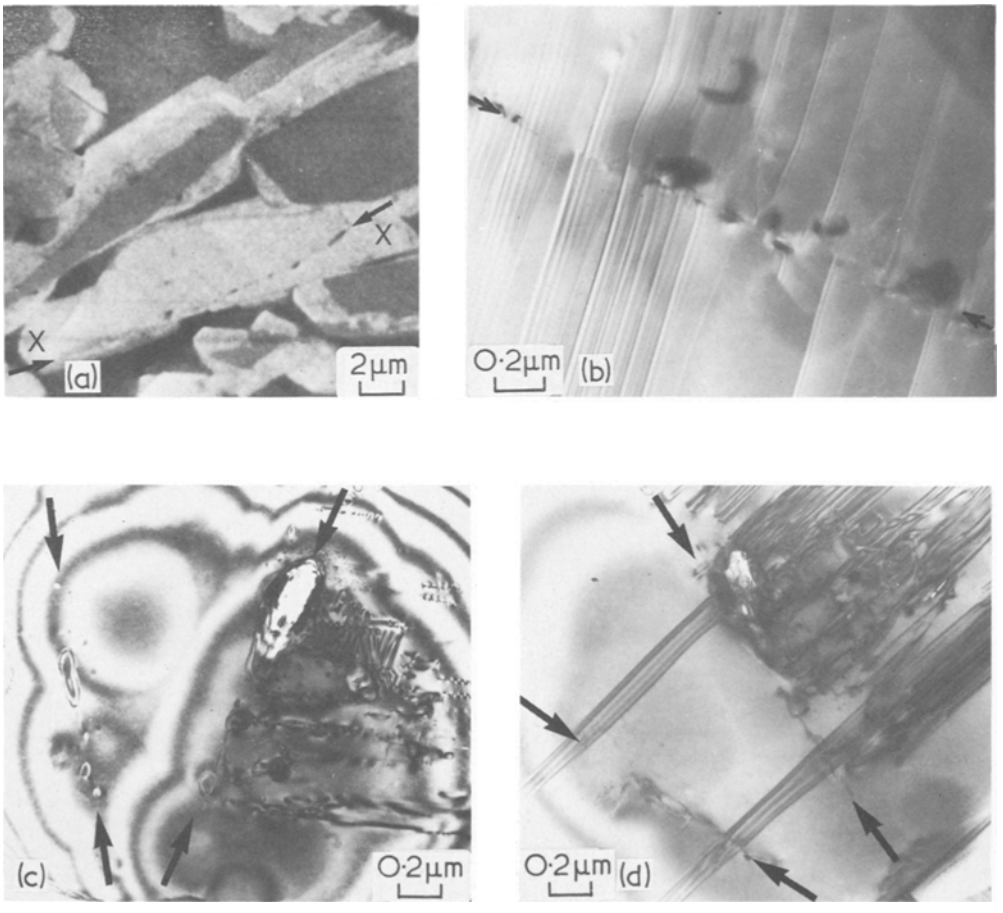

Figure 6 Poorly bonded epitaxial interfaces between the "old" and "new" parts of a single silicon carbide grain: (a) a scanning electron micrograph showing a poorly-bonded interface at X; (b) a transmission electron micrograph of a similar feature within one grain showing stacking faults crossing the interface and maintaining the same relative orientation; (c) a transmission electron micrograph of a grain containing a pair of internal boundaries seen as rows of pores or inclusions. The continuity of the depth fringes across the boundaries confirms the similar crystallographic orientation of the whole grain (two beam image, $g = 0\,0\,0\,1\,5$); (d) the same feature as shown in (c) tilted to show the continuous nature of the stacking faults crossing the interface, the faults being edge on in (c) (two beam image, $g = 1\,0\,\bar{1}\,1\,7$).

grains (similar to SC8 B, with typically smaller outer layers) but with additional finer mid-grey SiC grains distributed in the free silicon (Figs. 7c, d and e). The size of the outer (white) layer to the large grains was typically greater towards the outside of the cross-section, (although the number density of large grains did not appear to be significantly different), whilst towards the centre the amount of fine-grained SiC appeared to increase. Transmission electron microscopy also revealed the bimodal grain structure with an intimate mixture of large ($\sim 10\,\mu$m) and small ($< 1\,\mu$m) grains (Fig. 8a). The large grains were identified as being 6H or 15R with some faulting, whilst the finer-grained areas appeared to consist of small ($1\,\mu$m) β grains in a Si matrix (Figs. 8b and c). The bulk X-ray data (Table III) confirms that this batch contains a substantial percentage of 3C. Quantitative data on the proportion of angular grain cores in the total volume (Table IV) again shows a convincing fit to the value predicted (estimating the volume fraction of silicon from the X-ray data).

4.3. Isostatically pressed sheet (SC 12)

This material exhibited a very non-uniform microstructure (Fig. 9b) with several distinct types of localized features. Some regions resemble SC8 B,

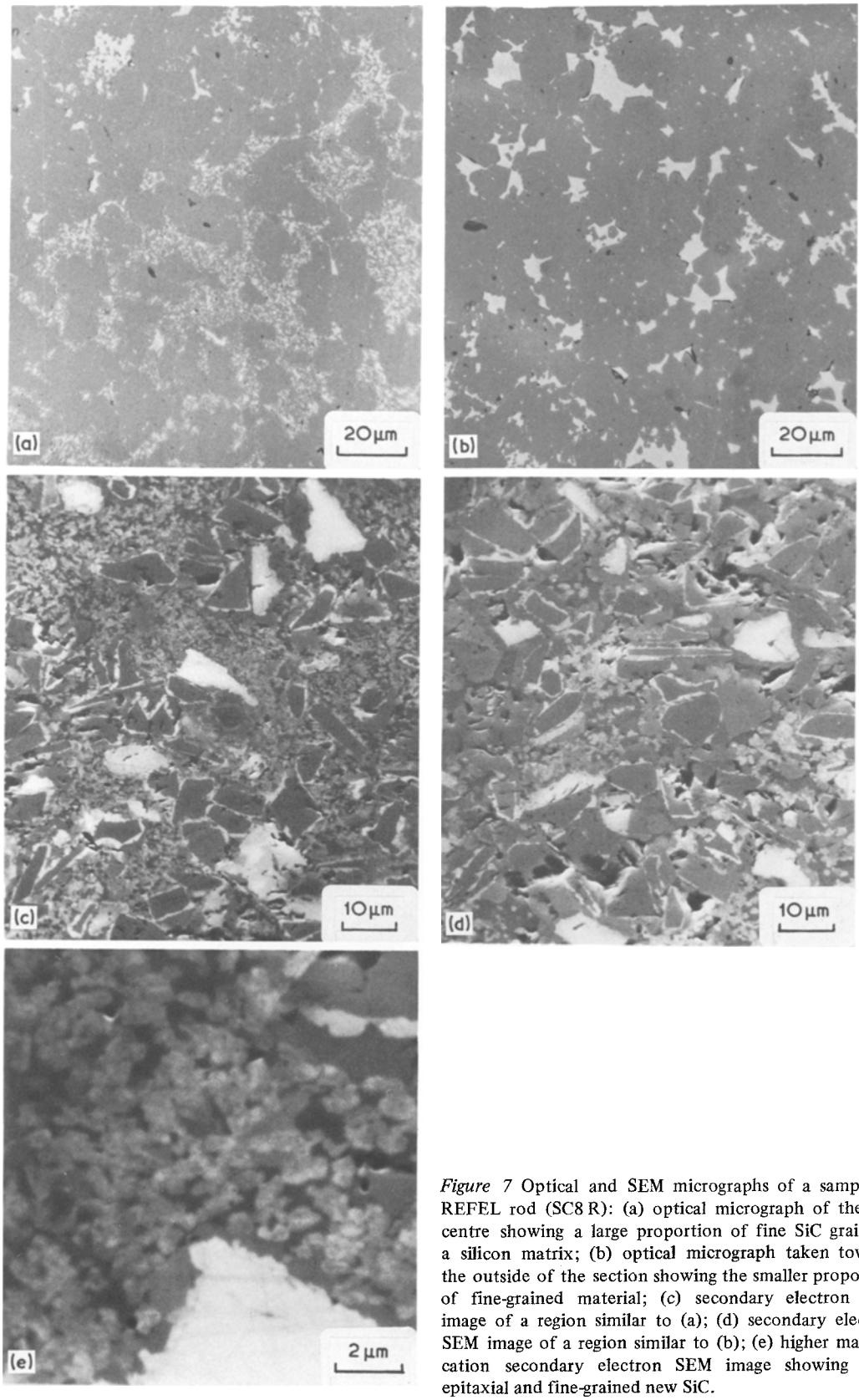

Figure 7 Optical and SEM micrographs of a sample of REFEL rod (SC8 R): (a) optical micrograph of the rod centre showing a large proportion of fine SiC grains in a silicon matrix; (b) optical micrograph taken towards the outside of the section showing the smaller proportion of fine-grained material; (c) secondary electron SEM image of a region similar to (a); (d) secondary electron SEM image of a region similar to (b); (e) higher magnification secondary electron SEM image showing both epitaxial and fine-grained new SiC.

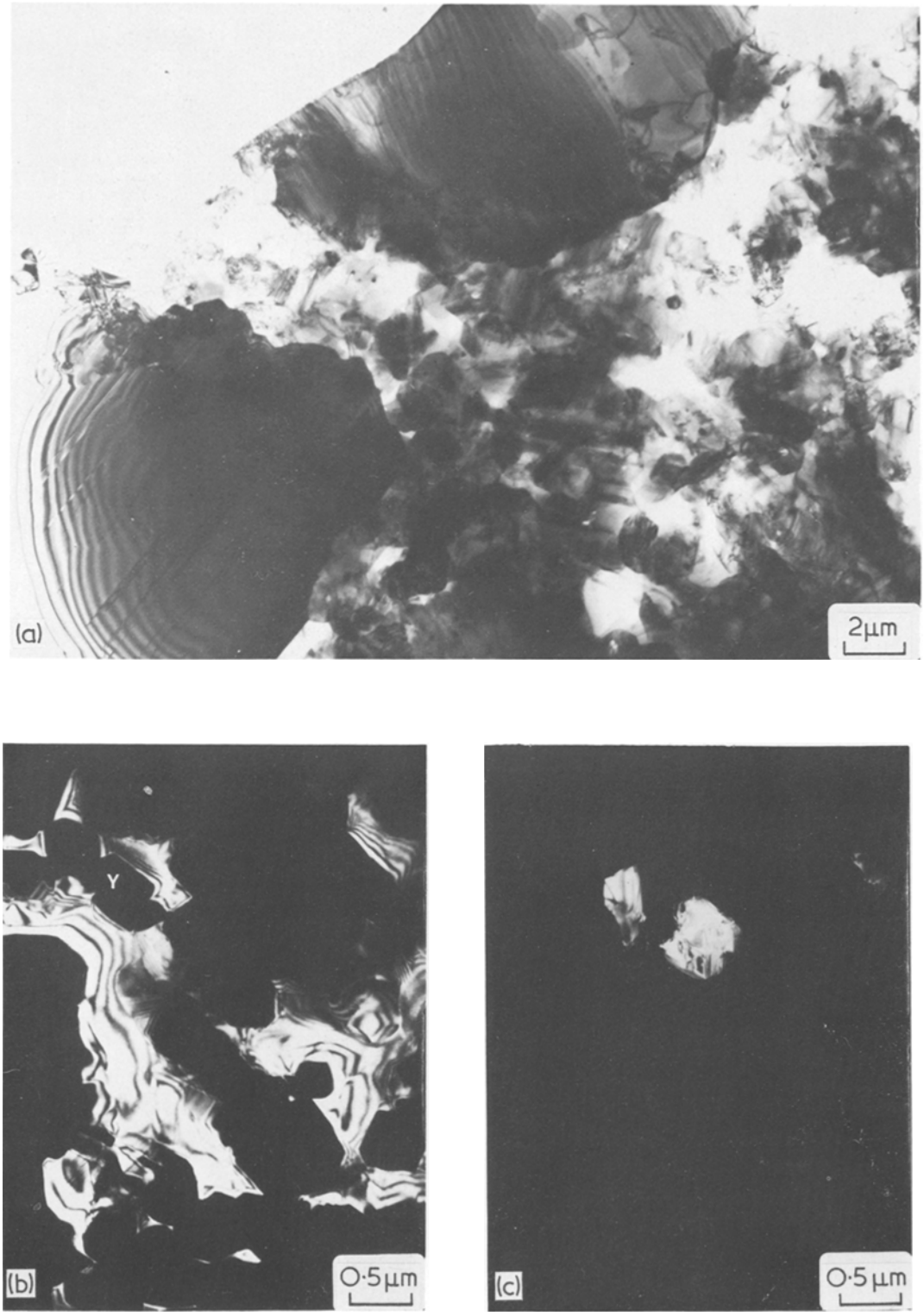

Figure 8 Transmission electron micrographs from the centre of the REFEL rod (SC8 R) showing (a) the bimodal SiC grain structure in bright field; (b) a dark-field image from the silicon matrix around the fine material and (c) a dark-field image taken using a reflection from the fine SiC material. The grains in (c) correspond to the location Y in (b) prior to tilting to the new diffracting condition.

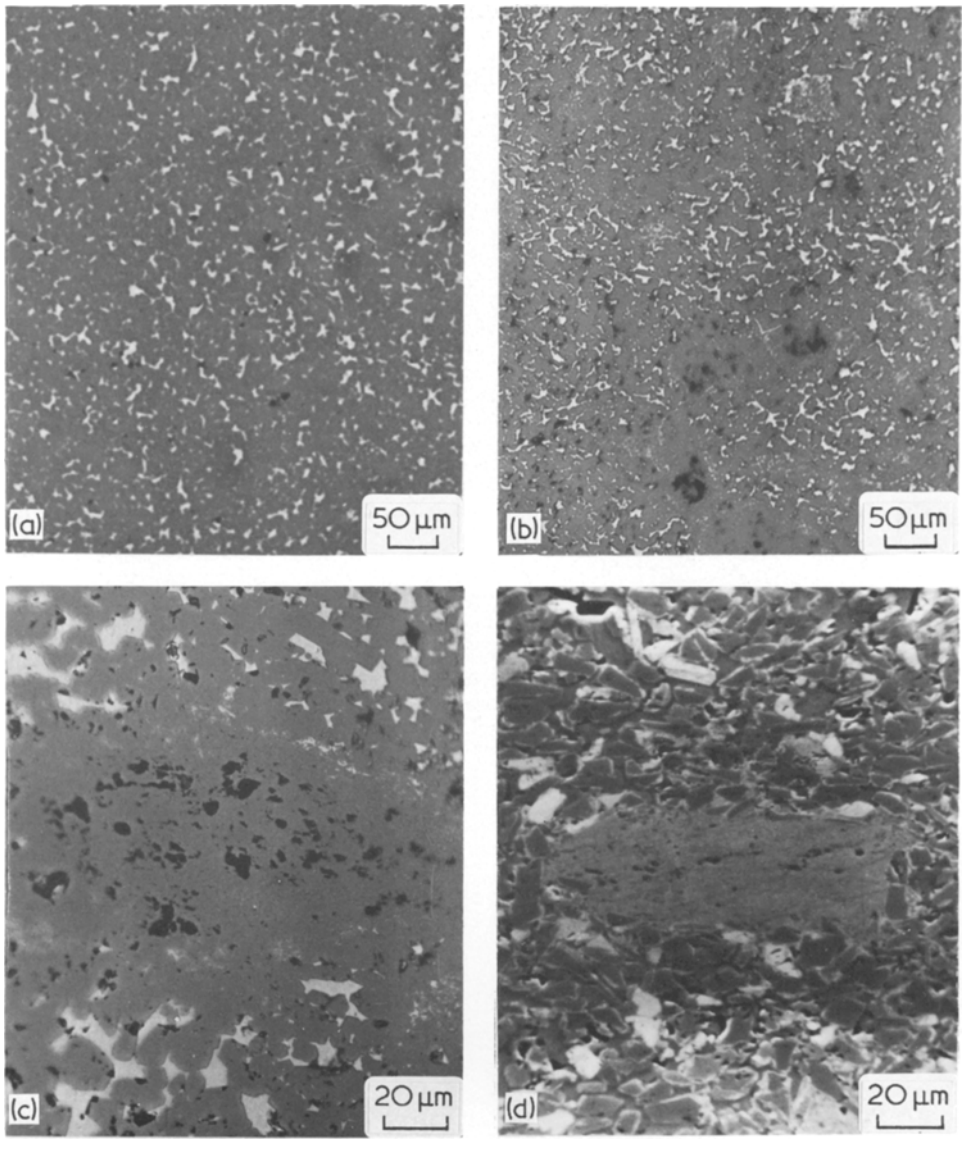

Figure 9 Micrographs comparing the microstructure of the pressed REFEL sample (SC12) with that of the bar (SC8 B). (a) Optical micrograph from the bar showing the uniform microstructure (c.f. Fig. 2); (b) optical micrograph from the pressed sample taken at the same magnification as (a) and showing the comparative inhomogeneity; (c) optical micrograph showing one of the characteristic featureless SiC "nodules" at higher magnification; (d) secondary electron SEM image of a region similar to (c) confirming the absence of any original SiC grains in the nodule.

others have the fine distribution of SiC in free Si similar to SC8 R, whilst in some other areas which appear as large ($\sim 100\,\mu m$) relatively featureless nodules on the SEM and optical micrographs (Figs. 9c and d), the structure is uniformly very fine and can only be resolved in the TEM (Fig. 10). Electron diffraction showed these regions to be largely very fine ($\sim 0.5\,\mu m$) SiC grains of the β-polytype and the bulk X-ray data confirmed the presence of significant amounts of 3 C material. Quantitative measurement (Table IV) indicated that the proportion of the total volume occupied by the featureless nodules was about 15%, which accounts for the majority of the 3C revealed by X-ray diffraction, whilst the proportion of angular grain cores in the silicon carbide was

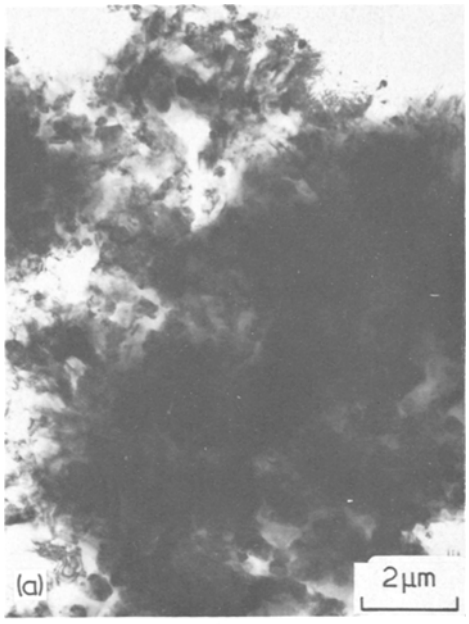

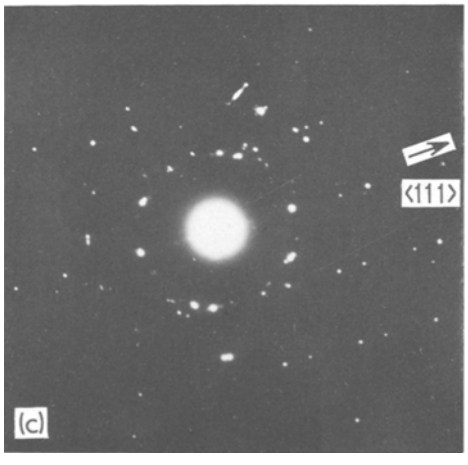

Figure 10 (a), (b) Transmission electron micrographs from one of the nodular features shown in Figs. 9c and d, showing the fine scale of the structure; (c) the predominantly β-SiC powder-like selected area diffraction pattern from a few of the SiC grains in the nodule.

substantially higher than in SC8 B, reflecting the higher proportion of silicon carbide in the original compact.

4.4. Extruded fuel can (SC 11)

Optical examination of this batch of material revealed the same general microstructural features as SC8 R, however the proportion of the finer-grained SiC was far less and did not vary systematically across the section, but in a random fashion. This sample of early material (about 1972) was examined to determine whether the discrepancy between the observed microstructure of, for example, SC8 B and that reported in the literature was due to some change in processing which had been introduced during the intervening period. Although the sample shape precluded complete characterization by subsequent TEM and X-ray diffractometry, optical (and particularly SEM) examination gave sufficient confirmation that the basic microstructural features were indeed the same.

4.5. Unseeded REFEL (SC 10)

Optical microscopy of this sample revealed a non-uniform microstructure (Fig. 11a) consisting of featureless nodules of silicon carbide in a matrix of finely distributed silicon carbide and silicon, the latter constituting about 75% of the total volume. In the SEM secondary electron images (Fig. 11b) the nodules showed up very slightly darker than the finely distributed silicon carbide, but did not reveal the angular shape characteristic of the darker material in other samples. The bimodal grain distribution was clearly observed in TEM, where the nodules were identified as

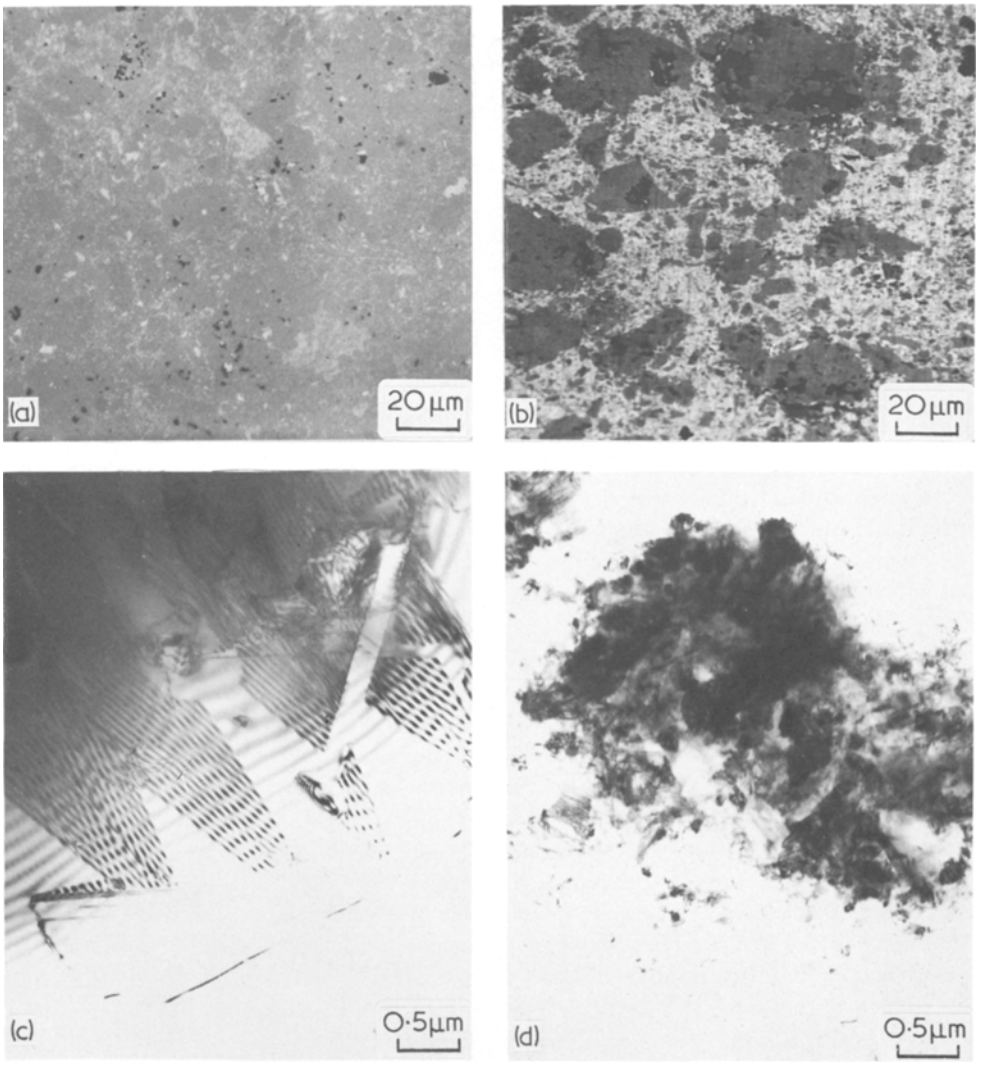

Figure 11 The microstructure of the unseeded REFEL SiC sample (SC10): (a) optical micrograph; (b) secondary electron SEM image taken at 5 kV to enhance the weak contrast) showing both coarse (darker) and fine (lighter) SiC and some residual silicon (black); (c), (d) transmission electron micrographs of the coarse-grained and fine-grained SiC regions. (c) exhibits both stacking faults and twins indicative of cubic (β) material, and this is confirmed by the corresponding diffraction pattern (Fig. 1b).

aggregates of a few β silicon carbide grains (Fig. 11c), each about 2.5 μm in diameter, whilst the polytype of the finer material (Fig. 11d) could not be identified by electron diffraction due to its very fine scale* (grain size ~0.1 μm).

The large β grains often contained stacking faults and twins on the {1 1 1} planes (see Fig. 11c). Bulk X-ray analysis indicated that the SiC in this sample was virtually 100% β.

5. Discussion

5.1. Microstructure of SC8 B

The microstructural observations on the extruded bar sample, SC8 B, (see Section 4.1) are clearly incompatible with previous descriptions of the microstructure of REFEL silicon carbide. Firstly, the evidence from both grain by grain electron diffraction and bulk X-ray diffraction, indicates that the proportion of β silicon carbide present is

*"Powder" patterns generally obtained by selected area diffraction techniques from these areas are almost impossible to characterize because of the similar intensity distributions from many of the polytypic structures (see Section 2.2).

very small, being no greater than that present in typical samples of α-SiC abrasive grit (e.g. carborundum 600 mesh) presumed similar to that used in the initial green compact [18]. Thus the silicon carbide formed during the reaction-bonding process must consist largely of hexagonal α polytypes, and shows a distribution of polytypes characteristic of material formed from the vapour phase at much higher temperatures (> 2000° C) [8, 19] than those attained during the "REFEL" process. Secondly, none of the microstructural investigations on this sample show any evidence of a fine-grained matrix, (β or otherwise), between the original α-SiC particles.

No distinction can be made between the new and old material by TEM or by optical or SEM (backscattered) examination of polished surfaces. However, contrast in secondary electron SEM images has allowed the original angular SiC particles to be located and distinguished from the newly-formed silicon carbide, which is seen to be distributed as a continuous layer of appreciable thickness around each of the original particles to make a composite grain, this identification being shown to be consistent with the known composition of the initial compact by quantitative microscopy. Since there is no fine-grained material present, this layer must either be a truly epitaxial overgrowth or alternatively consist of a few individual grains each 2 to 5 μm in diameter, but in either case the new material must have nucleated on the original particles since it always forms a continuous whole without intervening free silicon.

The information from TEM of thin foils does not allow these two similar resultant microstructures, occurring either independently or in conjunction, to be unambiguously distinguished, since, while TEM is indispensible for defect and local crystal structure analysis, and while pronounced grain size effects (e.g. a bimodal distribution) can be identified in images from thin foils, smaller variations in grain size distribution are difficult to determine in this way. This is due partly to the small sample volume thin enough for transmission and partly to the impossibility of deducing the true original shape and environment of thin remnants of grains bordering perforations. However, although most of the grains show no obvious variations in internal structure consistent with the observed secondary SEM contrast, some examples of poorly-bonded epitaxial interfaces have been observed between adjacent regions of crystal of identical orientation (Fig. 6) which probably correspond with "new"/"old" interfaces similar to that marked (X) in Fig. 6a.

From previous work [8, 20–22], on the precipitation of SiC from solutions of C in molten Si, it would be expected that material formed under the conditions of temperature and purity characteristic of the REFEL process should be of the β polytype. Consequently the observed formation of α polytypes is most likely to have been caused by the seeding effect of the original α particles, this hypothesis being strengthened by the observation that the distribution of polytypes is predominantly the same in both "old" and "new" material. Liquid phase epitaxy with solutions based on pure silicon melts has been previously observed to result in the growth of layers of identical polytype on α seeds [23], although some changes in α-polytype have also been observed [23, 24], the latter not being totally unexpected since the experiments were invariably carried out with growth perpendicular to the basal plane (i.e. the new material has no contact with the prior stacking sequence). However, the preferential growth direction has been observed to be parallel to the basal plane [25] (which allows this "edgewise" growth to maintain the original stacking sequence, as observed with vapour phase epitaxy by Powell and Will [26]), and thus, with no imposed restrictions on growth direction, the likelihood of seeding the exact stacking sequence around a pre-existing SiC grain is high.

Thus it is likely that the new material is an identically oriented epitaxial layer of the same polytype as the original particle, and this view is supported by the occasional observation, in backscattered SEM images, of channelling contrast between adjacent composite grains but never between old and new material within an individual composite grain. Positive identification of the orientation within specific areas of the composite grain was attempted using selected area channelling mode on a Cambridge S180 SEM but proved to be impracticable due to the fine scale of the microstructure, while attempts to obtain secondary electron images and diffraction patterns from the same grain in a thin foil using a JEOL 100C STEM were also unsuccessful because the secondary electron contrast between old and new material could not be observed with an ion-beam etched

thin foil, probably due to a considerable topographic signal. Epitaxial growth has previously been reported in a coarser-grained reaction-bonded SiC by Sato *et al.* [27], but, in contrast to the present observations, all the newly formed SiC was then claimed to be β, of which the epitaxial (β on α) material constituted but a small proportion, the remainder growing, independently, from the melt.

5.2. Distribution of impurities in SC8 B

The starting materials used in the REFEL process, although relatively pure, all contain similar small amounts of impurities (Table II), sufficient to cause a change in the secondary electron emission coefficient, δ, from the value for pure SiC by the mechanisms outlined in Section 3. Of these impurities, aluminium, for instance, is known [28] to create acceptor states in the band gap, and thus it is likely to be a principal cause of the observed variation in δ*. The diffusion distance for aluminium in silicon carbide [28] during the heating cycle experienced in the manufacturing process (the Acheson process [29]), for commercial α-SiC grits is of the order of 10 to 50 μm, and thus sufficient to ensure that each original grain has a uniform internal distribution and hence appears uniformly dark in the SEM image. However different grains from different parts of the furnace may differ in aluminium content. The grits are roughly graded by colour, which is also related to impurity content, and therefore any batch should consist largely of grains of similar impurity level, although some individuals may differ, thus probably accounting for the occasional "white"† grains observed in SEM images.

Typical diffusion distances during the heating cycle of the REFEL process [2] are, by contrast, very small ($\sim$150 Å) and consequently no appreciable solid state diffusion can take place. It has been observed [8] that the precipitation of silicon carbide from silicon melts is accompanied by rejection of impurities to the liquid such that the concentration may be as much as 10^2 to 10^5 times lower in the SiC than in the starting materials. Thus it is to be expected that the first new material formed immediately around an original particle of SiC will be much purer, and hence appear much lighter in shade in the secondary electron image, than the usually uniformly dark core. The boundary between the two will be sharp since the distance which impurities from the "old" particle, such as aluminium, can diffuse into the new material is only about 150 Å, which is near the resolution of the IIA SEM used‡. This limitation on solid state diffusion will also cause any local differences in the grown-in impurity content of the new material to be retained, leading to the generally less uniform observed secondary electron emission. In particular, the occurrence of dark contrast in the new silicon carbide adjoining a residual silicon region, which presumably was the last to be deposited, can be attributed to the higher impurity content of the melt from which it was precipitated.

This impurity distribution also accounts for the appearance of the typical etched microstructures as published by Kennedy *et al.* [4, 2] and Ashford [30]. which distinguish the "old" and "new" material by the difference in overall rate and local uniformity of etching. Several of the features on these etched microstructures were attributed to the presence of β-SiC, but in fact delineate the epitaxial layer of differing purity.

5.3. Microstructural variations

All the samples examined contained some new silicon carbide in the form of an epitaxial overgrowth, but in most cases there was additional finer-grained new material, the presence of which was always associated with the identification by X-ray diffraction of substantial quantities of β silicon carbide. The distribution of this fine-grained material as a dispersion in a silicon matrix indicates that it is unlikely to have nucleated on the original silicon carbide, and thus its stacking sequence would not be seeded by the α crystals. Therefore it is reasonable to infer that the finer-grained material consists entirely of cubic β-SiC deposited from the molten silicon on the graphite as has previously been reported by (for example) Beckmann [8]. In general the new silicon carbide could be deposited either on the

*Other impurities may contribute to the effect, but an insufficiency of published data about their diffusion rates and effects on the band structure makes it more difficult to relate their distributions to the observed contrast.

†The white "cores" may either be highly pure or contain impurities enhancing or not affecting δ.

‡Annealing experiments have shown that the broadening of this interface can be followed using impurity-controlled SEM contrast [13].

old silicon carbide or on the graphite, or on both, and the final microstructure will therefore be controlled by the relative availability of the two kinds of nucleation site and by the rates of nucleation and growth at each.

In the extreme case where no SiC is included in the original mix, as in sample SC10, all the silicon carbide formed is cubic, whereas the typical microstructure of REFEL, as observed both in the present study and in a reappraisal of previously published micrographs (e.g. in [2, 30, 31]), contains a large majority of epitaxially deposited α-polytypes with a small proportion of fine β dispersed in the silicon. It would be expected that initial compacts formed by pressing would be less well-mixed than those formed by extrusion, and this is reflected by the presence in the former of large regions without any original silicon carbide. This is apparently a characteristic feature since a previously published optical micrograph [32] of pressed REFEL also shows the non-uniformity of phase distribution observed (in SC12) during the present study. In those regions containing no SiC nuclei, all the new silicon carbide nucleates on the graphite due to the absence of any alternative site, thus producing the observed nodules of fine-grained β silicon carbide. The presence of these nodules and their size gives some indication of the scale over which the mass transport processes are effective during reaction-bonding, which must be considerably less than $\sim 100\,\mu$m, otherwise the nodule might be expected to be filled by epitaxial growth of the surrounding α-grains, yet greater than $\sim 1\,\mu$m otherwise epitaxial growth could never be the predominant mechanism as it is in most cases.

However in the type of region where there is a relatively uniform fine distribution of original silicon carbide particles to act as nuclei (and epitaxial growth predominates), it is still possible to have fine β-SiC nucleating on the graphite. An explanation of differences in the relative proportions of epitaxial and cubic material in these circumstances will depend on a thorough description of the reaction mechanism, which in turn requires detailed thermodynamic data, and information concerning the structure of the green compact. However some conclusions can be drawn, regarding the general nature of the mechanism, by observation of the final microstructures, and it seems likely that such variations are caused by local differences in the distribution of graphite and porosity in the green compact. The effects of external parameters (e.g. temperature) are unlikely to be the cause, since in general both mechanisms of deposition can occur in an apparently random fashion within an individual sample.

5.4. The effect of processing variables

It is desirable to have a very fine uniform distribution of porosity to increase the active surface area of the graphite, and hence the rate of the reaction, and to produce a uniform microstructure. This is achieved by using a very fine colloidal graphite, and consequently the local distribution of porosity will depend on how these fine particles are dispersed in the binder, which is dependent on both the efficiency of mixing of the constituents and on the homogenization effected during the shaping process. Assuming the initial mixing to be approximately constant, it would be expected that the porosity distribution would be finer and more uniform in an extruded compact than in a pressed one, and in the former case to be finer in a compact which has been reduced in diameter by a large amount. If the distribution is very fine this will tend to favour nucleation on the graphite for two reasons. Firstly, the larger graphite surface area provides a greater proportion of this nucleation sites, and secondly, the rate of solution of graphite will increase, thus increasing the local supersaturation and making the formation of a large number of nuclei more likely. Thus the rod (SC8 R), which has been reduced more in extrusion than SC8 B, shows an unusually high proportion of non-epitaxial new silicon carbide, whilst the pressed sample (SC12) shows the expected gross inhomogeneity leading to random differences in local microstructure even in those regions not denuded of original silicon carbide. The microstructural variation across the section in SC8 R is probably caused by the flow patterns in the extrusion process.

Thus it seems that β-SiC nucleates and grows on the graphite under conditions of either very poor or very good mixing of the original compact. In the former case it does so in local masses (nodules) due to the absence of any alternative nucleation site, while in the latter the more homogeneous

β distribution is due to the high surface area of the graphite*. The rest of the new SiC always grows epitaxially and, somewhere between the extremes of the two different β-producing compacts is the most favoured state for epitaxial nucleation and growth. This is important since it should be noted that in no case does the fine β material bond together the α grains, and thus the high temperature strength of the material would be expected to be governed primarily by the boundaries between impinging epitaxial growths which may well contain a film of unknown structure and composition. The presence of the fine β silicon carbide may, however, affect the mechanical properties in that it not only reduces the average size of the grains but also reduces the likelihood of any pair of adjacent α grains impinging. The overall effect is therefore difficult to predict. The silicon matrix also plays a vital part in controlling the strength at lower temperatures as is shown by the marked drop in strength at its melting point [2].

5.5. Summary of the reaction model

The modified reaction model can be summarized as follows. The molten silicon climbs by capillary action, moving most rapidly through the outer skin of the compact which has a larger average pore size due to the "burn-out" effect [2], and thence infiltrating radially towards the centre. Some graphite dissolves in the silicon and is precipitated as silicon carbide either on the α-SiC particles or on the graphite depending on the availability of local nucleation sites. The associated evolution of heat causes the local temperature to rise and thus accelerates the rate of dissolution of graphite and causes the reaction to proceed rapidly to local completion. Mass transport will take place by diffusion of carbon in the molten silicon down the activity gradient from the sources of carbon (i.e. the graphite particles) to the nucleation sites, and, since it is unclear whether most heat is evolved at the site of dissolution or that of precipitation, this may in some cases even involve transport up the local temperature gradient. As the silicon front climbs, the reaction zone moves upwards and the compact is progressively converted to silicon carbide, the reaction zone at any one time being confined to a narrow band just behind the liquid front which can be observed as a zone of locally high temperature [2]. The presence of a gross temperature gradient between the reaction zone and the material immediately below it probably has no direct effect on the reaction mechanism since the cooler region must already be virtually completely converted to silicon carbide and the gross mass transport effects (by convection) reported by Beckmann [8] will almost certainly be inoperative in the present case where the silicon is distributed in a network of capillaries (c.f. the $\sim 100\,\mu$m limit deduced in Section 5.3).

6. Conclusions

Several samples of REFEL silicon carbide have been examined using a wide range of microstructural techniques and it has been observed that the silicon carbide formed during the reaction-bonding process may be deposited either as an epitaxial layer of α on the original α-SiC grit or as a fine dispersion of β-SiC nucleated on the graphite. The relative abundance of nucleation on these two sites has been shown to vary from sample to sample, and some suggestions have been made as to the processing variables which probably affect the final microstructure on account of their effect on the distribution of SiC, graphite and porosity (i.e. binder) within the initial green compact. The reaction model of Forrest *et al.* [2] has been modified to account for some of the microstructural variations observed and it seems apparent that the direct effect of the gross temperature gradient on the local reaction mechanism is not as important as previously thought, and is certainly not as simple. In addition it has been suggested that the fine β-SiC does not contribute significantly to the bulk strength of the material which is held together by interfaces between impinging epitaxial growths and by a silicon matrix.

Acknowledgements

The authors would like to thank the European Research Office of the US Army for financial support, UKAEA Springfields for providing the materials, and Professor R. W. K. Honeycombe for provision of laboratory facilities. GRS also gratefully acknowledges a maintenance grant from ERO. Mr M. Naylor helped obtain the quantitative

*The importance of the scale of the graphite distribution on the morphology of the new SiC has also been established by unpublished work carried out at UKAEA [33].

metallography data quoted in Table IV, as an undergraduate research project, and thanks are also due to J. Ward and G. Mitchell for technical assistance with the Quantimet and X-ray diffractometer respectively. The authors would also like to acknowledge useful discussions with N. W. Jepps, P. Kennedy and J. Ware.

References

1. P. POPPER, "Special Ceramics" (Heywood, London, 1960) p. 209.
2. C. W. FORREST, P. KENNEDY and J. V. SHENNAN, "special Ceramics 5" (British Ceramic Research Association, Stoke-on-Trent, 1972, p. 99.
3. C. W. FORREST and P. KENNEDY, "Special Ceramics 6" (B. Ceram. R. A., 1975) p. 183.
4. P. KENNEDY and J. V. SHENNAN, Atom. No. 206 (1973); also reprinted in "Silicon Carbide 1973" (see reference 24) p. 359.
5. C. A. BROOKES and M. IMAI, "Special Ceramics 1964" (Academic Press, London, 1965) p.251.
6. C. R. GOSTELOW and J. E. RESTALL, *Proc. Brit. Ceram. Soc.* **22** (1973) 117.
7. J. J. BURKE, A. E. GORUM and R. N. KATZ (Editors), "Ceramics for high performance applications", (Brook Hill, Chestnut Hill, Mass. USA 1974).
8. G. E. J. BECKMANN, *J. Electrochem. Soc.* **110** (1963) 84.
9. L. S. RAMSDELL, *Amer. Min.* **32** (1947) 64.
10. O. O. ADEWOYE, G. R. SAWYER, J. W. EDINGTON and T. F. PAGE, U.S. Army Tech. Report DAJA-37-74-C-1310 (1974).
11. O. O. ADEWOYE, PhD Thesis, University of Cambridge (1976).
12. O. O. ADEWOYE and T. F. PAGE, in preparation (1978).
13. G. R. SAWYER, T. F. PAGE and R. J. PARGETER in preparation (1978).
14. J. WARE (UKAEA, Springfields) private communication.
15. P. T. B. SHAFFER, *Acta Cryst.* **B25** (1969) 477.
16. A. H. GOMES de MESQUITA, *ibid*, **23** (1967) 610.
17. A. van der ZIEL, "Solid State Physical Electronics", (Prentice-Hall Inc., New Jersey, USA, 1968) p. 84.
18. N. W. JEPPS, private communication.
19. H. N. BAUMANN, *J. Electrochem. Soc.* 99 (1952) 109.
20. R. W. BARTLETT, W. E. NELSON and F. A. HALDEN, *ibid* **114** (1967) 1149.
21. R. C. ELLIS, "Silicon Carbide", Proceedings of the Conference in Boston, 1959 (Pergamon Press, London, 1960) p. 124.
22. F. A. HALDEN, *ibid*, p. 115.
23. R. W. BRANDER and R. P. SUTTON, *J. Phys. D.* 2 (1969) 309.
24. W. von MUENCH and K. GILLESSEN, "Silicon Carbide–1973", Proceedings of the Conference in Miami Beach (University of South Carolina Press, Columbia, South Carolina USA, 1974) P. 51.
25. K. GILLESSEN and W. von MUENCH, *J. Cryst. Growth* 19 (1973) 263.
26. J. A. POWELL and H. A. WILL, *J. Appl. Phys.* **44** (1973) 5177.
27. H. SATO, S. SHINOZAKI, M. YESSIK and J. E. NOAKES, "Silicon Carbide–1973", Proceedings of the Conference in Miami Beach (University of South Carolina Press, Columbia, South Carolina USA, 1974) p. 222.
28. Y. A. VODAKOV and E. N. MOKHOV, *ibid*, p. 508.
29. A. R. VERMA and P. KRISHMA, "Polymorphism and polytypism in crystals" (J. Wiley Inc., London and New York 1966) p. 93.
30. J. P. ASHFORD, "Special Ceramics 4" (British Ceramic Research Association, Stoke-on-Trent 1968) p.173.
31. P. MARSHALL, *ibid* p. 191.
32. A. F. McLEAN, R. R. BAKER, R. J. BRATTON and D. G. MILLER, U.S. Army Tech. Report AMMRC CTR 76-12 (ARPA) (Watertown, Mass. 1976).
33. P. KENNEDY (UKAEA, Springfields), private communication.

Received 19 July and accepted 2 August 1977.